Numerical Acoustics
31265

Technical University of Denmark

Numerical approach to a Schroeder Sound Diffuser in a Room

Ali Borhan-Azad s192760
Alexander Kittel s164010
Miguel Cuadrado Sierra s193504

Jan 2021

Contents

1 Goal

Our project is centered around the quadratic residue Schroeder diffuser (QRD), a type of number-theoretic diffuser invented by Manfred R. Schroeder. This type of diffuser is composed of a series of wells of varying depths, and works by causing a mixture of phase shifts on the incident wave in order to diffuse reflected sound. The design process of a QRD is based around the following formula for the depth of the wells:

$$\text{depth}_\text{n} = \frac{\lambda_d}{2N} n^2 \cdot \text{mod}(N), \tag{1}$$

for a given prime number N, lower cutoff wavelength λ_d and $n = 0, 1, ..., N-1$. The efficient diffusion range of the QDR is fully defined by the geometry of the wells, with the width giving us the high cutoff half-wavelength for head-on incidence. Designing and building QRDs is mostly done empirically, and an investigation into the effects of these decisions constitutes the motivation for this project.
The goal of this project is a parametric analysis of the effects of a QDR on the sound pressure field of a room through a programmatic approach. Our approach is centered around the boundary element method (BEM), and makes use of the OpenBEM toolbox for MatLab.

2 Theory

2.1 Boundary Element Method

Boundary element method (BEM) is a numerical method used to solve partial differential equations. Only the boundary is discretized, and the integral equations are solved for the boundary. The solution in the domain, interior or exterior, can then be determined from the boundary solution.
In the acoustic application, the sound pressure field must satisfy the Helmholtz equation, according to a set of boundary conditions:

$$\nabla^2 \hat{p} + k^2 \hat{p} = -\hat{Q}(\underline{y}), \tag{2}$$

where $\hat{p}$ is the complex pressure amplitude at the point $\underline{y}$, k is the wavenumber. The elementary solution to the Helmholtz equation is called the Green's function. The Green's function describes the sound field at $\underline{y}$ caused by a point source at a location $\underline{x}$,

$$\nabla^2 G(\underline{x}, \underline{y}) + k^2 G(\underline{x}, \underline{y}) = -\delta(\underline{x} - \underline{y}), \tag{3}$$

where $G(\underline{x}, \underline{y})$ is the Green's function and $\delta(\underline{x} - \underline{y})$ represents the point source.
There are numerous solutions for the Green's function, which should be chosen

between according to their suitability to the problem. For example, in an infinite, isotropic medium,

$$2D: \; G(\underline{x}, \underline{y}) = \frac{e^{-jkR}}{4\pi R} \tag{4}$$

$$3D: \; G(\underline{x}, \underline{y}) = \frac{j\pi}{2} H_0^{(1)}(kR), \tag{5}$$

where $R = \left|\underline{x} - \underline{y}\right|$ and $H_0^{(1)}(kR)$ is the zeroth order Hankel function of the first kind.
Multiplying the homogeneous Helmholtz equation, eq. 2 with $\hat{Q}(\underline{y}) = 0$, gives

$$\int_V (\nabla^2 \hat{p} + k^2 \hat{p}) G \, dV = 0, \tag{6}$$

which, after some simplification, results in the Helmholtz integral equation (HIE),

$$\int_S (\hat{p} \frac{\partial G}{\partial n} - G \frac{\partial \hat{p}}{\partial n}) \, dS = - \int_V \hat{p} (\nabla^2 G + k^2 G) \, dV. \tag{7}$$

This leads to a set of integral equations to be solved on the discretized boundary, and is also used to determine the domain solution from the boundary solution. [1] [2]

2.2 Physical Properties of the Problem

One of the aims of placing a QRD in a room is to reduce the standing wave patterns produced by sound reflections in phase, by means of introducing extra path and phase differences. Therefore the room modes are expected to be affected by the QRD, and this may be apparent in a frequency response analysis.
Additionally, when a room mode is diminished by the effect of the QRD, the spatial coherence of the sound field is expected to increase, when the nodal lines and peaks of pressure at specific places in the room disappear. Thus, the standard deviation of the sound pressure within the room can be seen as a metric to assess the diffusivity of the room.
As it was stated, a QRD is defined by its well width w_d (design wavelength-dependent), its order N and its fin width. Since λ_d represents the lowest cut-off wavelength for diffusion, the effect of QRD is expected to be apparent at frequencies above the cut-off frequency $f_d = c/\lambda_d$.

Due to the limited amount of time available to investigate the topic, we decided to reduce the scope of the analysis to the well width. Besides, the room dimensions were fixed to $l_x = 4$ m and $l_y = 3$ m.

The frequency response was studied for four different widths: $0.137 \cdot \frac{\lambda_d}{4} = 5$ cm, $0.137 \cdot \frac{\lambda_d}{2} = 10$ cm, $0.137 \cdot \lambda_d = 20$ cm and $0.2 \cdot \lambda_d = 29$ cm. They analyzed frequency band is [200,400] Hz, a range below the modal density starts to be important in this room.
Additionally, a higher frequency full field solution is obtained, using a N = 11 QRD with a $f_d = 450$ Hz and $w_d = 0.137\lambda_d$.

2.2.1 Physical modelling approach

The entire room is modeled as a series of segments defined in a clockwise manner, with the diffuser itself integrated in the bottom wall. The process of drawing up the geometry is largely iterative, with each well of the diffuser defined individually as a series of segments and connected to the larger structure one by one.
For testing our model, we have opted with a pressure point source within the room. This is both simple to implement and mirrors real-life well enough for our purposes. Solving for the pressure field in the room, we use a mesh with 6 elements per wavelength of the source. This mesh is designed to overlap with the QDR so that we can get the solutions within the diffuser wells. We can approximate the room frequency response by taking the mean of a smaller set of points in the field solution, similar to using a series of measurement microphones.
The wall opposite to the diffuser is designed with a nonzero admittance in order to avoid excessive energy in room modes. The method chosen to include the room losses was the Delany-Bazley impedance model. Specially suited for porous materials, it gives the surface admittance in terms of the flow resistivity of its effective flow resistivity, σ_e [3]. In our case, a value of $\sigma_e = 3 \times 10^4$ $\mathrm{N\,s\,m^{-4}}$ was chosen for the top wall, a typical Rockwool value [4]. The rest of the walls were set as acoustically hard. An example plot of our setup, along with source position and point probes can be seen in fig. 1.

3 Verification of the model

It is important to verify that the numerical model used gives trustworthy results. With this purpose, its performance was analyzed when applied to a simplified 2D cavity with the same dimensions of the one used in the problem, $l_x = 4$ m and $l_y = 3$ m. The aim was to obtain, using the model, the different room modes of the cavity when it is excited with a point source at the frequencies predicted by the equation [5]

$$f_{mn}^{2D} = \frac{c}{2}\sqrt{\left(\frac{m}{l_x}\right)^2 + \left(\frac{n}{l_y}\right)^2}. \tag{8}$$

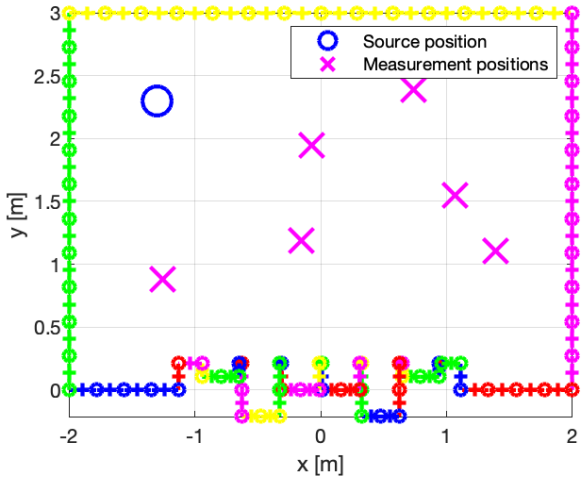

Figure 1: Example layout for testing the effects of a diffuser on the sound field. Each straight line is considered a segment and is composed of a series of nodes used for solving the system. In this exaggerated version, the node density is much lower for visual clarity. Note the randomized position of the probes for the frequency response and standard deviation calculations.

The first 9 modes and their orders are lsted in Table 1.

The sound pressure inside the cavity was obtained considering the walls of the room as the body surface. For the field points, a mesh of points filling the interior of the surface was defined. The surface generated with the BEM 2D segment generator can be seen in fig. 2.

It is important to notice that the interior mesh of the room was constructed starting from a small distance of the wall. This was done in order to reduce the influence of near-singularities due to a calculation very close to a boundary [6].

The sound pressure level obtained for the first nine analytically predicted resonance frequencies are shown in fig. 3. It can be seen that they resemble quite well to the expected shapes of room modes, see Table

4 Convergence

An inevitable consequence of numerical methods is truncation errors. That is, the difference between the numerical result and the true or analytical result. The scale of this error is dependent on the level of discretization in the model. A convergence study is performed in order to find a level of discretization which will result in a satisfactorily small truncation error while avoiding unnecessarily expensive computations.

(m,n)	**f (Hz)**
(1,0)	42.99
(0,1)	57.33
(1,1)	71.66
(2,0)	85.99
(2,1)	103.35
(0,2)	114.66
(1,2)	122.46
(3,0)	128.99
(3,1)	141.16

Table 1: Room modes of a 2D cavity with $l_x = 4$ m and $l_y = 4$ m, obtained from the 8. It can be seen that they fit well with the shapes of the modes obtained with the numerical model.

Ideally, the convergence of the numerical result to the true result should be studied. In this case, however, there is no analytical solution to compare to, nor are there measured data. Therefore, the convergence towards the result with a very fine level of discretization was studied. The assumption is made that this finely discretized model provides results that are very close to the true solution.
The convergence study was carried out as follows. A line of equally spaced field points was defined inside the room. The boundary solution was determined for a number of discretization levels, and for each of these the complex pressure amplitudes at the field points was found. For each discretization level, the truncation error was then defined as

$$\Delta p_i = \frac{\int_C |p_i - p_{fine}|^2 \, dx}{\int_C |p_{fine}|^2 \, dx}, \tag{9}$$

where p_i is the pressure for the i^{th} discretization level, p_{fine} is the reference pressure from the very finely discretized model.

Figure 4 shows the convergence to a finely discretized solution for two frequencies: 200 Hz and 400 Hz, the minimum and maximum frequencies for which the frequency responses in section 6 are calculated. It is evident that at higher frequencies, a finer discretization is required to achieve errors in the same order of magnitude. This is expected since it is known that higher frequencies correspond to shorter wavelengths, thus more points are needed to correctly identify the pressure behaviour. This is accounted for in the results presented subsequently, as the minimum mesh density is defined according to the highest frequency of interest.

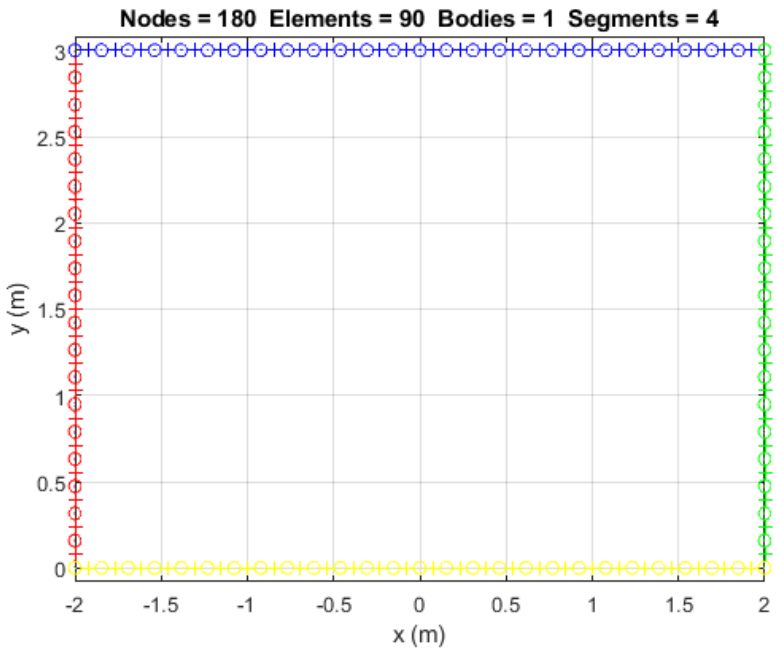

Figure 2: Geometry of an rectangular empty room generated with OpenBEM 2D for verification purpose. Each segment has 6 elements per wavelength of the excitation. The upper segments is designed with a flow resistivity $\sigma_e = 3 \times 10^4$ N s m^{-4}. The rest are acoustically hard.

5 Sensitivity

In this section, the sensitivity of the model to slight variations in the width of the separating fins is investigated. A QRD can be designed to high precision using simulations, but in reality, production will have tolerances. As a case study, it is assumed that there is a production tolerance of 5 mm in the fin width. An order seven QRD was modelled, with a design frequency equal to a resonance, approximately 233 Hz. The well width was set to $0.137\lambda_{design}$, Schroeder's suggestion for the maximum well width [7]. The design fin width was 2 cm, hence the production wavelength was 2 cm $\pm$ 5 mm. Therefore, frequency responses and pressure deviations were calculated for the three fin widths: 15 mm, 20 mm and 25 mm.

The results of this are shown in figure 5. At high and very low frequencies, there is very little effect. Of interest is a region beginning at approximately the design frequency, 233 Hz, and ending at approximately 270 Hz. In this region, the fin width variation leads to a clear variation in the response. This could suggest that the model is more sensitive in the region immediately following the design frequency, however further investigation would be needed to fully identify

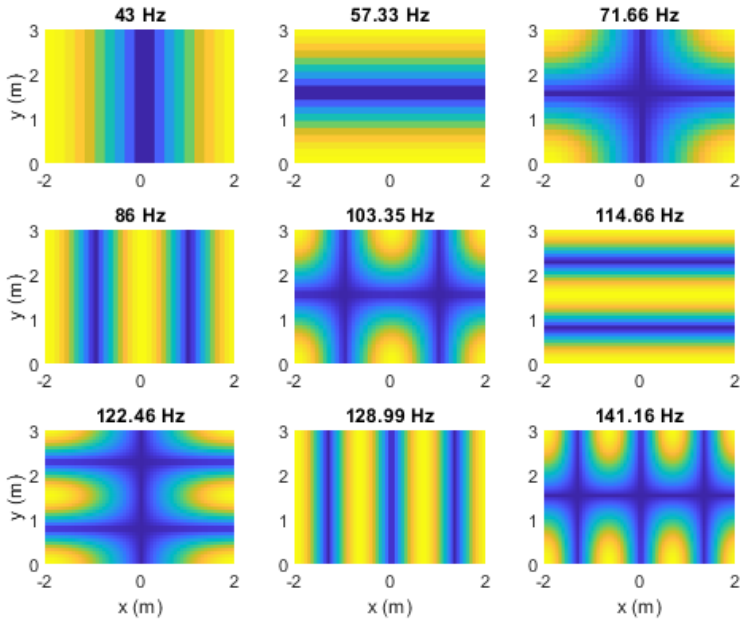

Figure 3: Room modes for a $l_x = 4$ m and $l_y = 3$ m cavity, obtained with the BEM model. The room is excited with a point source at $P_s = (1.5\text{m}, 2.5\text{m})$ at the frequency predicted by equation 8. The aim is to verify that the simple room modes are obtained with the numerical model used in the QRD problem.

the causes.

6 Results

6.1 Field solution

A side-by-side comparison of the pressure field in the room with the QRD and without can be seen in fig. 6. The point source emits at 700 Hz (chosen randomly), and the result is computed for a minimum of 8 points per wavelength for both the boundary and the field solutions. Because of the computational load associated with higher frequencies, only one set of parameters was investigated for this frequency. The results show the diffuser has a very large effect on the soundscape of the room at the tested frequency, eliminating the modal behaviour that could be observed in the verification setup.

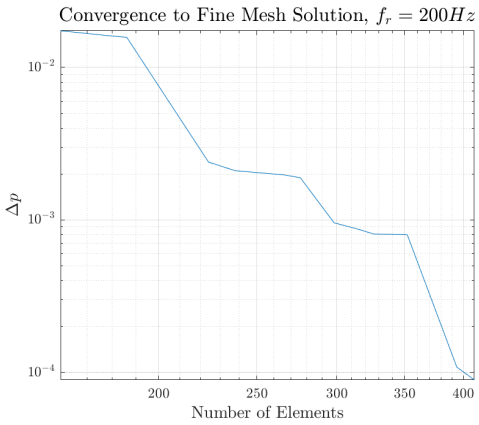

(a) The convergence to a finely discretized solution with 546 boundary elements, performed for an excitation frequency of 200 Hz.

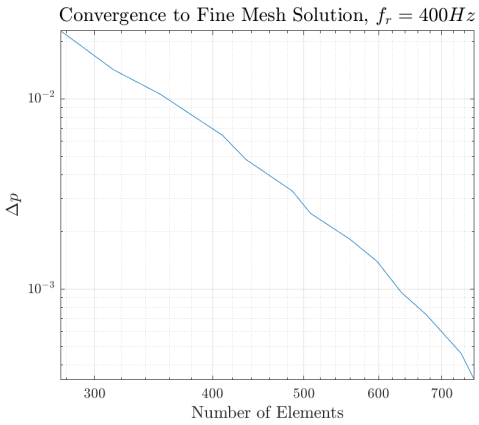

(b) The convergence to a finely discretized solution with 1,052 boundary elements, performed for an excitation frequency of 400 Hz.

Figure 4: The convergence to a finely discretized solution performed for two excitation frequencies: (a) 200 Hz and (b) 400 Hz, the minimum and maximum frequencies for which the frequency responses in section 6 are calculated.

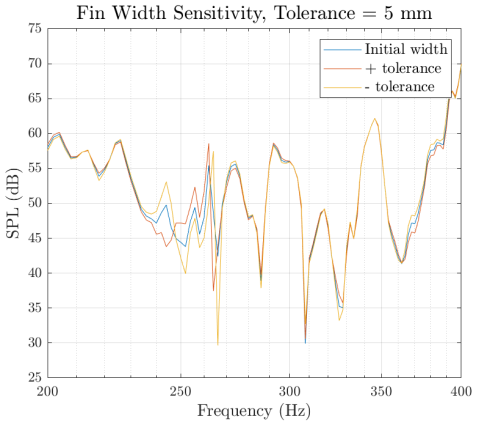

(a) The frequency response of the room when the QRD fin width is varied by a manufacturing tolerance.

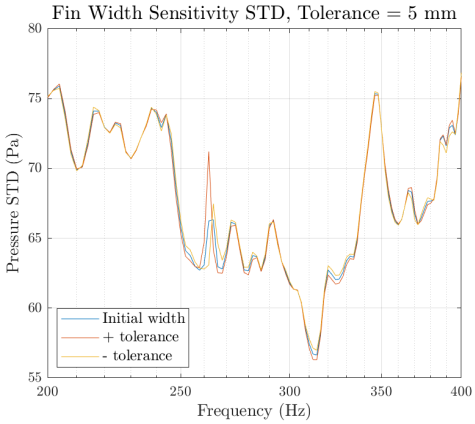

(b) The pressure deviation in the room when the QRD fin width is varied by a manufacturing tolerance.

Figure 5: The frequency response of and pressure deviation in the room when the QRD fin width is varied by a manufacturing tolerance. The initial fin width is set to 2 cm, with a tolerance of 5 mm. The QRD is of order 7, with a well width of $0.137\lambda_d$.

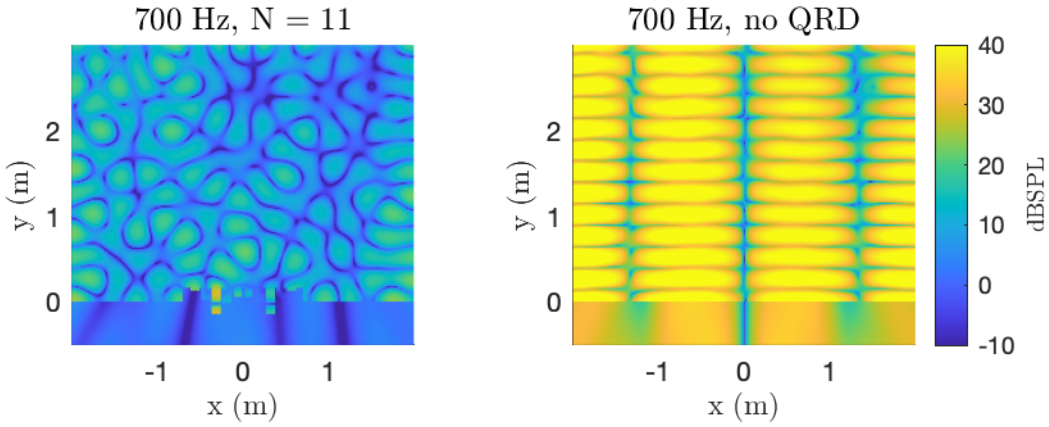

Figure 6: Sound field simulation for a 700 Hz point source located near the top right corner. On the left, a room with a QRD of order 11, designed for frequencies above 450 Hz. The well width is set to $0.137\lambda_d$ for this setup. On the right, the same room configuration but without the QRD. Both plots have the same colorscale.

6.2 Frequency analysis

The frequency response is a useful quantitative measurement in room acoustics. When an empty room is excited with a point source, the frequency response would show the room modes in the analyzed frequency bandwidth. If the room geometry is modified or obstacles are place in it, the frequency response is expected to show deviations from the empty situation.
As it was mentioned before, only one QRD order is studied, N = 7, with a designed frequency $f_d = 233$ Hz; and four different well widths were analyzed: 5 cm, 10 cm, 20 cm and 29 cm. This choice has been done following the recommendation found in [7]. Each setup can be seen in fig. 7.

6.2.1 Broadband frequency response analysis

The frequency response of sound pressure level and spatial standard deviation is shown in fig. 8 to fig. 11, comparing the QRD and the empty room situation.

It can be seen that the SPL when the QRD is in the room shows some gaps at specific frequencies as well as new peaks at frequencies different from the empty room modes, specially above the f_d. This behaviour seems to intensify when the width is increased. However, some modes remain unchanged in both situations.

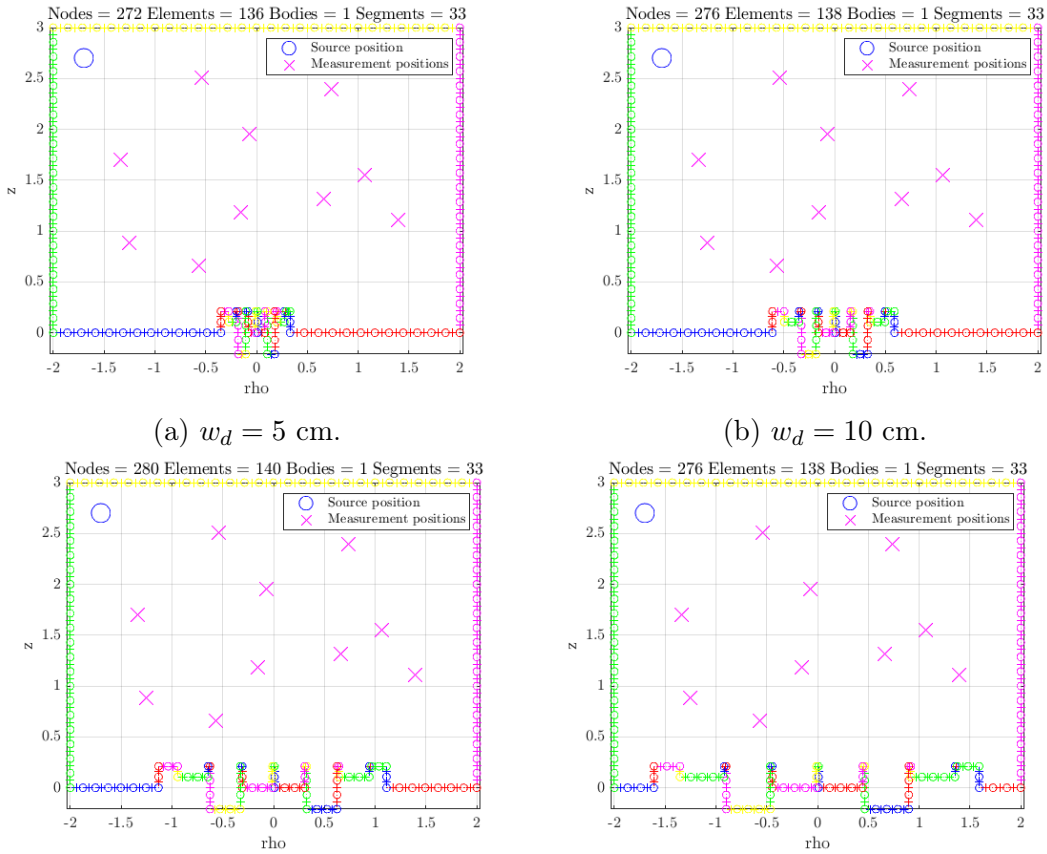

(a) $w_d = 5$ cm. (b) $w_d = 10$ cm.

(c) $w_d = 20$ cm. (d) $w_d = 29$ cm.

Figure 7: Four different setups analysed, corresponding to four different well widths: a) 5 cm, b) 10 cm, c) 20 cm, d) 29 cm. X: Measuring positions. ◯: Source Position.

The extreme case of a very wide QRD shows a quite different response than the empty case.

Regarding the spatial standard deviation, it can be seen that at some frequencies corresponding to the empty room modes σ_{xy} decreases, meaning that the spatial correlation increases when the QRD is in, e.g. 350 Hz with $w_d = 5$ cm and $w_d = 10$ cm. Conversely, σ_{xy} increases or shows a shifted behaviour towards higher frequencies at other regions, this being more apparent for the two widest QRD wells.

This behaviour might be explained attending to the physical effects of the QRD in the room. When sound waves hit the diffuser, they are reflected in different directions, producing a different response that will depend on frequency. Those modes that present a high geometry in the axis perpendicular to the diffuser will

be more affected and may be cancelled. At the same time, the reflections may produce new constructive and destructive interference with other waves reflected in the room that were not produced in the empty room situation.

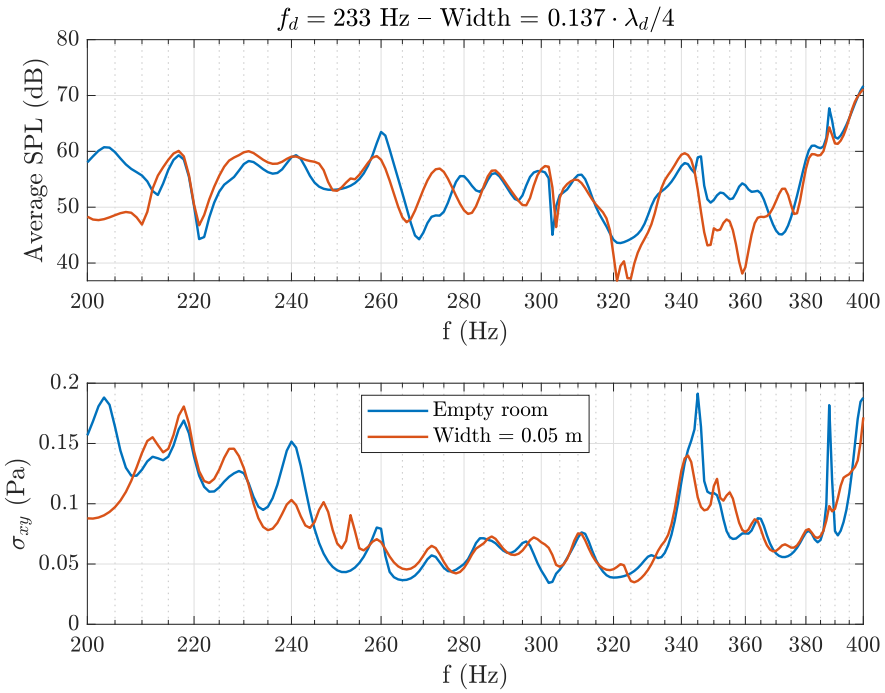

Figure 8: Average sound pressure level (top) and standard deviation of sound pressure (bottom) computed over 10 randomly chosen points in the room in two different conditions: an empty room and a room with a QRD of $w_d = 5$ cm placed in one wall, see fig. 7, top left.

6.2.2 Narrowband frequency response analysis

Deepening in the effect of the QRD in the room modes, a higher resolution analysis is shown in fig. 12. We chose the frequency range [330, 360], centered in the room mode at 346 Hz, to analyze the effect of each QRD width. It is apparent that a width of both 5 cm and 10 cm breaks the mode and the sound field becomes more diffuse. On the other hand, 20 cm and 29 cm produce an increase in the average sound pressure level within a frequency range of ~ 10 Hz centered in 346 Hz, and fails in increasing the spatial correlation.

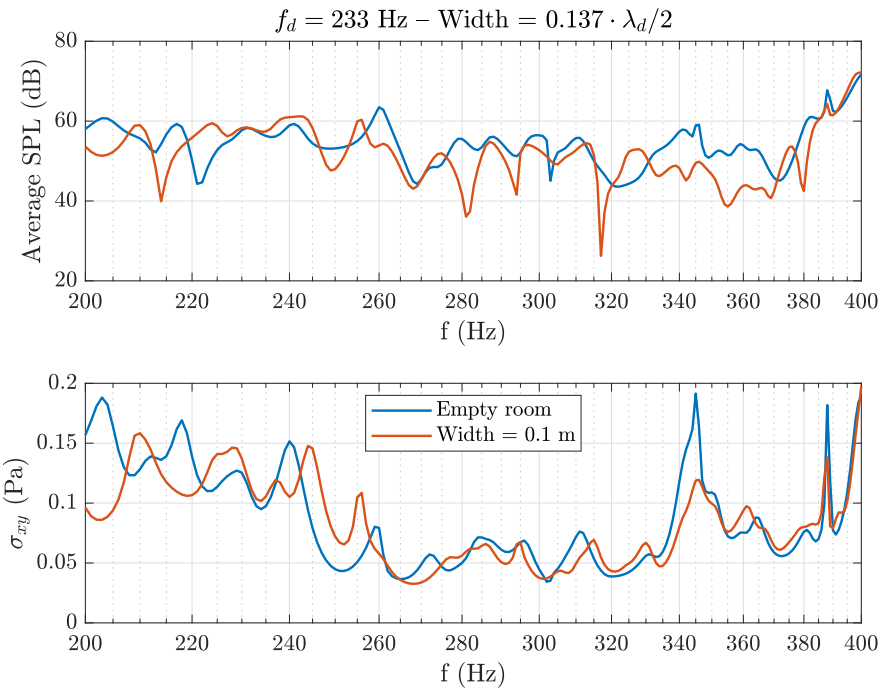

Figure 9: Average sound pressure level (top) and standard deviation of sound pressure (bottom) computed over 10 randomly chosen points in the room in two different conditions: an empty room and a room with a QRD of $w_d = 10$ cm placed in one wall, see fig. 7, top right.

7 Conclusion and further work

Within the constraints of this course, our project has demonstrated a method for simulating the effects of a variable QRD on the pressure field in a room. However, more investigations can be done to refine this method, both for the sake of better results, but also in optimizing the approach.
Firstly, the field mesh being computed should be truncated, so that the points existing outside the diffuser aren't computed (see fig. 6 for an example of this behavior). This must be done in a way that depends on the iterative geometry, so that the mesh can adapt to different QDRs. Second, including an extra dimension would allow a true simulation of a room in 3D, though the best way to implement this would likely be through the Finite Element Method (FEM). Most of the pitfalls of FEM are also avoided by this being a fully contained interior body problem. We would then also be able to extend the scope of the investigation to include different types of diffusers such as corner diffusers etc.

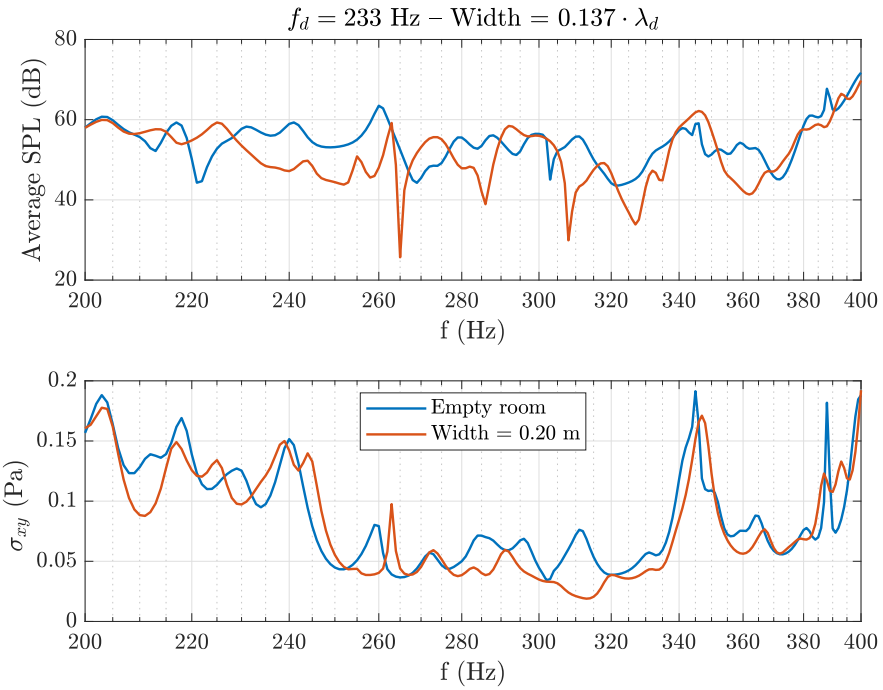

Figure 10: Average sound pressure level (top) and standard deviation of sound pressure (bottom) computed over 10 randomly chosen points in the room in two different conditions: an empty room and a room with a QRD of $w_d = 20$ cm placed in one wall, see fig. 7, bottom left.

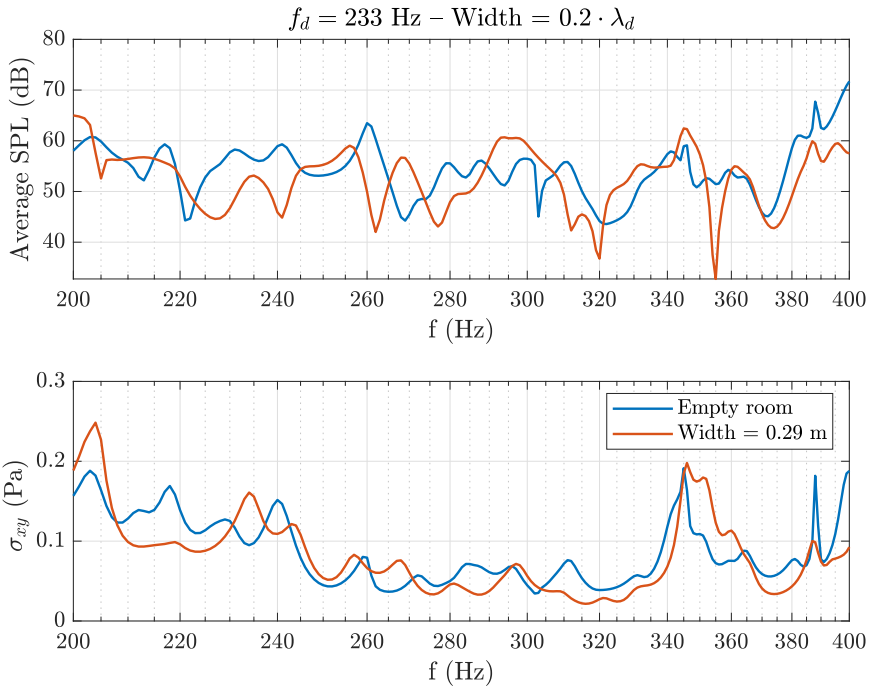

Figure 11: Average sound pressure level (top) and standard deviation of sound pressure (bottom) computed over 10 randomly chosen points in the room in two different conditions: an empty room and a room with a QRD of $w_d = 29$ cm placed in one wall, see fig. 7, bottom right.

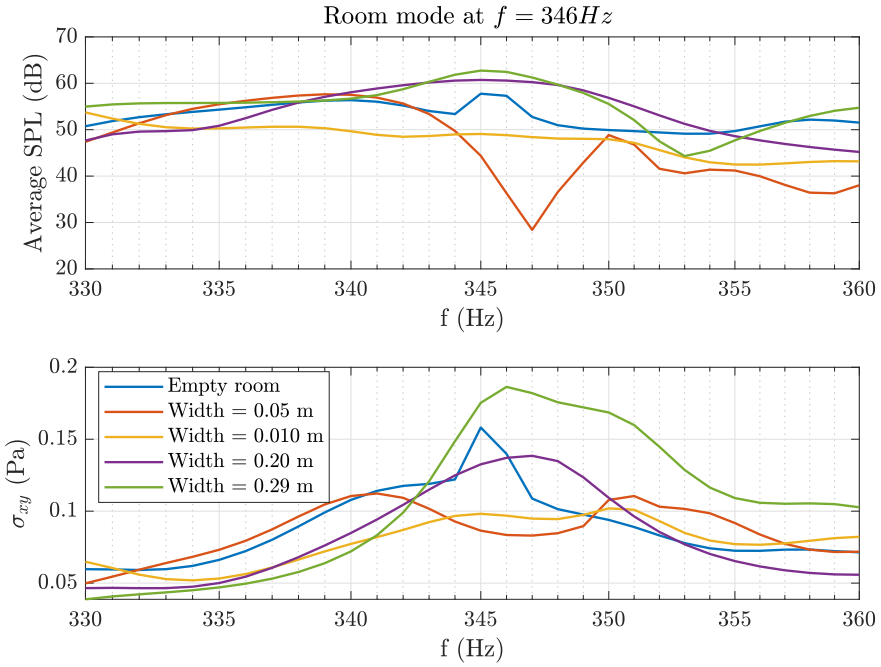

Figure 12: Average sound pressure level (top) and standard deviation of sound pressure (bottom) computed over 10 randomly chosen points in the room with four different QRD widths: 5 cm, 10 cm, 20 cm and 29 cm.

References

[1] N. Atalla and F. Sgard. *Finite Element and Boundary Methods in Structural Acoustics and Vibration*. CRC Press, 2015. ISBN: 9780429190285.

[2] V. Henriquez. "Lecture 3, Introducyiion to the Boundary Element Method". In: *Numerical Acoustics* (Jan. 2121).

[3] Gunnar Taraldsen. "The Delany-Bazley Impedance Model and Darcy's Law". In: *Acta Acustica united with Acustica* 91 (Jan. 2005), pp. 41–50.

[4] Jochen Schulz. *Rock wool, glass wool, hemp - which material is best suited for absorbers?* Mar. 2020. URL: https://www.jochenschulz.me/en/blog/rockwool-glasswool-hemp-best-absorber-material.

[5] F. Jacobsen and P.M. Juhl. *Fundamentals of General Linear Acoustics*. Wiley, 2013. ISBN: 9781118636176. URL: https://books.google.es/books?id=Sq6uFqlHg1gC.

[6] Jacobsen Cutanda Henríquez Juhl. "On the modeling of narrow gaps using the standard boundary element method". In: *JASA* 109 (2001).

[7] T.J. Cox and P. D'Antonio. *Acoustic Absorbers and Diffusers: Theory, Design and Application*. Taylor & Francis, 2009. ISBN: 9780203893050. URL: https://books.google.dk/books?id=f19%5C_6NFg4jkC.

A Computation time and mesh density

Throughout the project, we have had issues with our implementation of BEM in the sense that it would compute points outside of our defined geometry. To see if this could be due to using too coarse a mesh, we attempted a single computation for 20 points per wavelength, with our source at 700 Hz (meaning over 300,000 points in the field mesh). The QRD parameters are the same as in fig. 6 for comparison sake. The total computation time was over 6 hours, and generated close to 8 GB of data in total. Considering the result in fig. 13 is indistinguishable from that in fig. 6, we can safely say it would be wasteful to compute this level of mesh density.

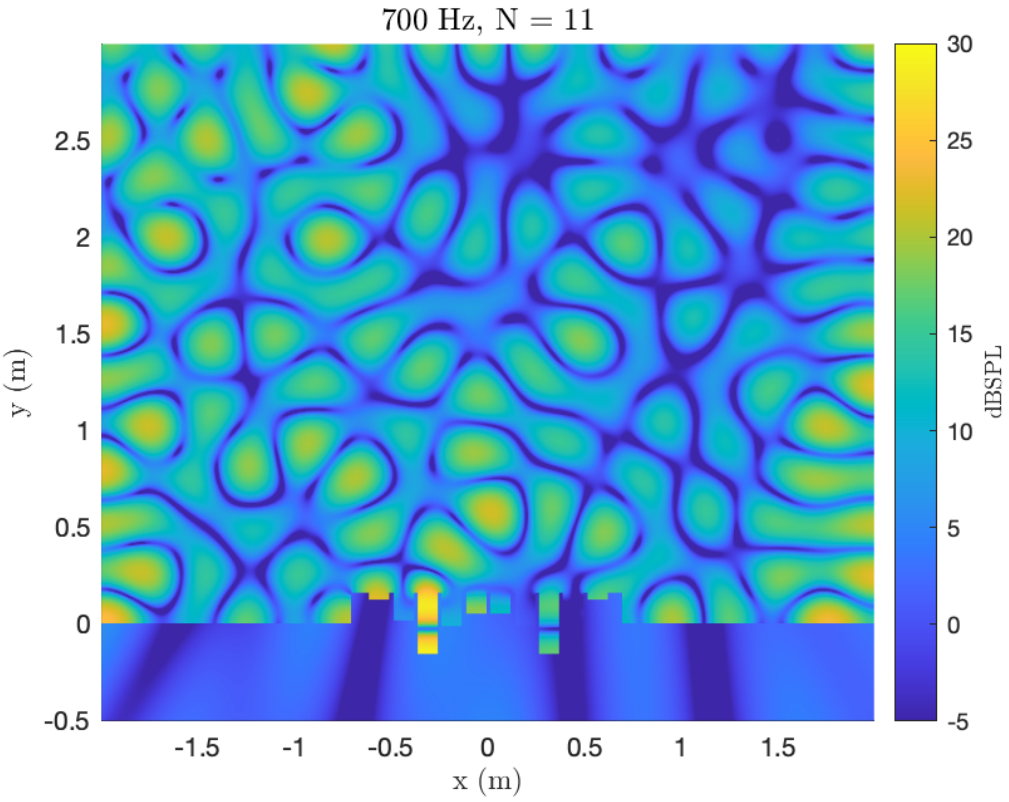

Figure 13: Very high mesh density pressure field solution for a QRD of order 11 designed for a lower cutoff of 450 Hz. The well width is set to $0.137\lambda_d$. The same issues arise behind the QRD wall, where our model shouldn't be able to compute different pressure values.